224/1-28-81

C

R 1517

DE 2238

LBL-6497
UC-11

Lawrence Berkeley Laboratory

UNIVERSITY OF CALIFORNIA

Engineering & Technical Services Division

MASTER

AEROSOL ANALYSIS FOR THE REGIONAL AIR POLLUTION STUDY - FINAL REPORT

J.M. Jaklevic, R.C. Gatti, F.S. Goulding, B.W. Loo, and A.C. Thompson

May 1980

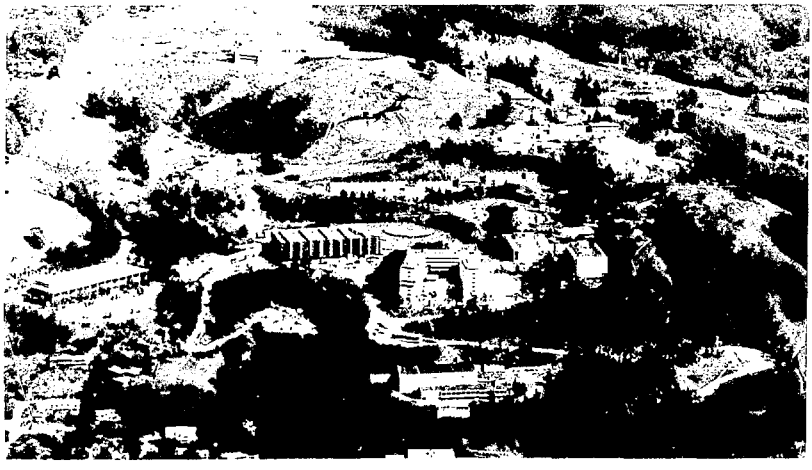

Prepared for the U.S. Department of Energy under Contract W-7405-ENG-48

DISTRIBUTION OF THIS DOCUMENT IS UNLIMITED

DISCLAIMER

This report has been reviewed by the Environmental Sciences Research Laboratory, U.S. Environmental Protection Agency, and approved for publication. Approval does not signify that the contents necessarily reflect the views and policies of the U.S. Environmental Protection Agency, nor does mention of trade names or commercial products constitute endorsement or recommendation for use.

This report was prepared as an account of work sponsored by the United States Government. Neither the United States nor the Department of Energy, nor any of their employees, nor any of their contractors, subcontractors, or their employees makes any warranty express or implied, or assumes any legal liability or responsibility for the accuracy, completeness or usefulness of any information, apparatus, product or process disclosed, or represents that its use would not infringe privately owned rights.

This report was done with support under an interagency agreement with the Department of Energy and Environmental Protection Agency. Any conclusions or opinions expressed in this report represent solely those of the author(s) and not necessarily those of The Regents of the University of California, the Lawrence Berkeley Laboratory or the Department of Energy, nor does mention of trade names or commercial products constitute endorsement or recommendation for use.

ABSTRACT

We describe the design and operation of an aerosol sampling and analysis program implemented during the 1975-1977 St. Louis Regional Air Pollution Study. A network of ten samplers were operated at selected sites in the St. Louis area and the total mass and elemental composition of the collected particulates were determined. Sampling periods of 2 to 24 hours were employed. The samplers were capable of collecting aerosol particles in two distinct size ranges corresponding to fine (<2.4 μm diameter) and coarse (>2.4 μm diameter) particles. This unique feature allowed the separation of the particulate samples into two distinct fractions with differing chemical origins and health effects.

The analysis methods were also newly developed for use in the St. Louis RAPS study. Total particulate mass was measured by a beta-particle attenuation method in which a precision of $\pm$ 5 μm/cm^2 could be obtained in a one minute measurement time. Elemental compositions of the samples were determined using an energy dispersive x-ray fluorescence method in which detectable limits of 5 ng/cm^2 or less were routinely achieved for elements ranging in atomic number from Al to Pb.

The advantages of these analytical methods over more conventional techniques arise from the ability to automate the measurements. During the course of the two year study, a total of more than 35,000 individual samples were processed and a total of 28 concentrations measured for each sample.

CONTENTS

Abstract iii
Figures vi
Tables vii
Acknowledgements viii

1. Introduction. 1
2. Aerosol Sampling Procedures 2
3. Mass Measurements 8

Relative humidity effects. 10
Atomic number dependence 10
Filter porosity effects. 12

4. X-Ray Fluorescence Measurements 14

Sensitivity. 14
Precision and accuracy 14
Calibration accuracy 25
Reproducibility of results 31

5. Data Handling 38

References 45

FIGURES

Number		Page
1	Map of the St. Louis area showing the location of 10 RAMS sites equipped with dichotomous samplers.	3
2	Diagram showing a typical installation of dichotomous samplers in the RAMS stations.	4
3	Cut point behavior and loss characteristics of the virtual impactor. The quantity A is the amount collected on the coarse filter; B the fine.	5
4	Cross section of beta gauge apparatus	9
5	Mass gain of 4 mg/cm^2 cellulose membrane as a function of % relative humidity	11
6	Minimum detectable limit for X-ray fluorescence analysis compared with average aerosol concentration ranges.	17
7	Voltage dependence of X-ray yield in X-ray fluorescence unit. Vertical line on curve represents normal operating voltage. . . .	19
8	Cross section of secondary fluorescence geometry.	20
9	Scans of sensitive region of X-ray fluorescence unit.	21
10	Diagram of spectrum stripping procedure	24
11	Illustration showing matrix absorption effects (A) and large particle attenuation (B).	30
12	Flow chart showing the overview of sampling, analysis and data merging.	37

TABLES

Number		Page
1	Summary of Sites, Times, and Intervals for which Particulate Data are Available	6
2	Atomic Number Dependence of Beta-Gauge Mass Attenuation Coefficient	12
3	Operating Conditions for Sampling and Analysis	15
4	Sensitivity for Energy Dispersive X-Ray Fluorescence Analysis	16
5	Calibration Solutions for Thin Aerosol Deposited Standards	27
6	Summary of Calibration Measurements	29
7	Particle Size Attenuation Corrections for the Light Elements (Adapted from Reference 14)	32
8	Reproducibility of Air Samplers Measured by Side-by-Side Sampling	33
9	Root Mean Square Deviations of Analyses of Identical Samples Over a Three-Month Period	34
10	Comparison of our Analyses with Independent XRF Measurements by R. Giauque	36
11	Sequence of Calculations Performed on Original X-Ray Fluorescence Results	40
12	Format for Data Tape Containing the Dichotomous Sampler Data for the Regional Air Pollution Study[a,b,c]	42
13	Interpretations of Status Words	44

ACKNOWLEDGMENTS

There are a number of people in the Instrumentation Development Group who have made significant contributions to the project over the past two years. D. Landis, R. Adachi, N. Madden, J. Meng, B. Jarrett, W. Searles and others have made significant contributions to the design and implementation of the hardware. J. Llacer is responsible for much of the computer programming used in the data handling.

We acknowledge the technical advice and assistance of T. Dzubay and R. Stevens of EPA. R. Giauque and his associates at LBL have assisted in the calibration of the X-ray fluorescence instrumentation. R. Fischer and his associates have done an admirable job of atttending to the around-the-clock operation of the analysis equipment.

SECTION 1

INTRODUCTION

Beginning in May, 1975 and continuing through April, 1977 a total of 35,000 individual ambient aerosol samples were collected at ten selected sampling sites in St. Louis as part of the St. Louis Regional Air Pollution Study (RAPS). The samples consisted of membrane filters on which the coarse and fine particulate fractions were collected separately using automatic dichotomous air samplers. The samples were returned to Lawrence Berkeley Laboratory (LBL) for analysis following collection at the field sites.

The program within the laboratory involved the determination of total mass by a beta-particle attenuation method. This required measurement of tare weights for each individual filter before being sent to the field sites and subsequent measurement on their return. A total of 70,000 mass measurements have thus been performed using an automated data acquisition and storage system. Elemental analysis of the particulate samples was performed for 27 elements using energy dispersive X-ray fluorescence analysis. Optimal sensitivities were obtained using pulsed excitation, and automated data handling was employed to facilitate the 35,000 data sets.

The original data from both the beta-gauge measurements and the X-ray fluorescence analyses are stored on magnetic tape. A large disk-oriented data storage system is used to merge the two data sets and incorporate the relevant sampling information. The data are then ordered according to station number and time and made available for the final output magnetic tapes. At the time of the data processing, corrections were applied to the original data to compensate for particle size effects, interelement interferences, cross contaminations between particle sizes and any other experimental artifacts which must be removed. The final data tapes have been submitted to EPA—Environmental Science and Research Laboratory—where they are available for correlation with other data sources in the RAPS study.

The following sections of this report will discuss in detail the procedures used in the aerosol sampling and analysis, and in data processing and validation. References are given to more detailed publications concerning the individual projects which constitute various phases of the program including dichotomous samplers,[1,2] X-ray fluorescence methods,[3,4] and beta-gauge techniques.[5]

SECTION 2

AEROSOL SAMPLING PROCEDURES

The sampling sites are stations in the St. Louis Regional Air Monitoring System (RAMS) which have been modified to accept the automatic dichotomous samplers developed and constructed by LBL in previous programs.[6] Ten RAMS sites were selected and equipped with these samplers. Figure 1 is a map showing the location and station number of the selected sites. Figure 2 illustrates the manner in which the automatic dichotomous samplers were installed. A 2.54 cm diameter isokinetic probe was connected to a 10 cm diameter manifold which projects vertically through the roof of the station. The manifold was equipped with a 30 cm diameter, cylindrical wind shield as shown. An additional rain shield covers the top.

The 1064 l/m flow was maintained by a cyclone-type blower. The 50 l/m flow required for the dichotomous sampler was maintained by a carbon vane pump internal to the sampler.

The automatic dichotomous sampler was equipped with a two-stage virtual impactor which separates the incoming particles into two size fractions above and below 2.4 μm aerodynamic diameter. The coarse and fine particle size fractions are then collected separately onto 1.2 μm pore size cellulose ester membrane filters. These 37 mm diameter filters are individually mounted in 5.0 x 5.0 cm plastic holders which are carried in a standard 36-slide projector cartridge. The use of the cartridge for the automatic handling of the samples eliminates contamination and reduces possible sources of operator error in the sequencing and ordering of the samples for shipment to and from the analysis laboratory.

The characteristics of the dichotomous sampler are illustrated in Figure 3. The cutpoint D_{50} (particle diameter at which 50% of the particles are collected on the coarse particle filter) was measured to be 2.4 μm. The cut characteristics are sharp with a ratio of D_{84} to D_{50} of 1.10. The solid particle losses are quite low. The maximum losses occur near the 2.4 μm cutpoint, which corresponds to the normal minimum in the urban aerosol size distribution[7]. The upper particle size cutoff for the coarse particle fraction was determined by the inlet configuration and has geen estimated to be 20 m.

As evident in the characteristics shown in Figure 3, a small fraction (5%) of the fine particle mass is collected as a part of the coarse particle fraction. The remaining 95% of the fine particles are collected on the other filter. Correction for this 5% interference between size fractions is made at the time of the final data processing (see Table 11).

Constant flow rate within the sampler was maintained by monitoring the pressure differential between the inlet and the second stage of the virtual impactor, (i.e., across the inlet orifices). This pressure differential is maintained constant by adjusting a variable impedance orifice included in the pump circuit as part of a feedback-loop. The flow calibration has an accuracy of ± 2% for room temperature air, with a repeatability of 0.5%. Periodic checks on the samplers indicated that the flow calibration remained constant to within 1% over the two-year duration of the study.

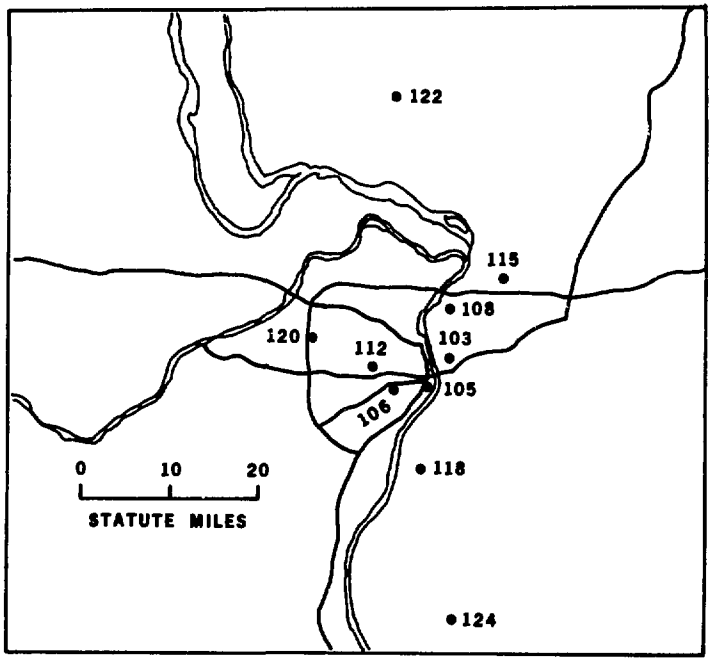

XBL 764-1126

Figure 1. Map of the St. Louis area showing the location of 10 RAMS sites equipped with dichotomous samplers.

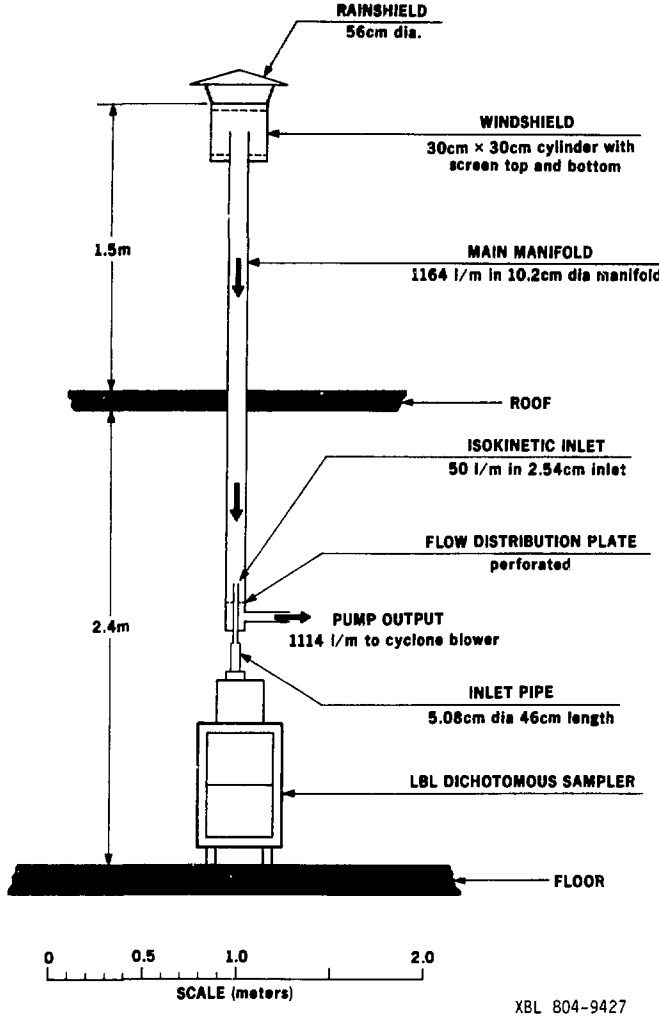

Figure 2. Diagram showing a typical installation of dichotomous samplers in the RAMS stations.

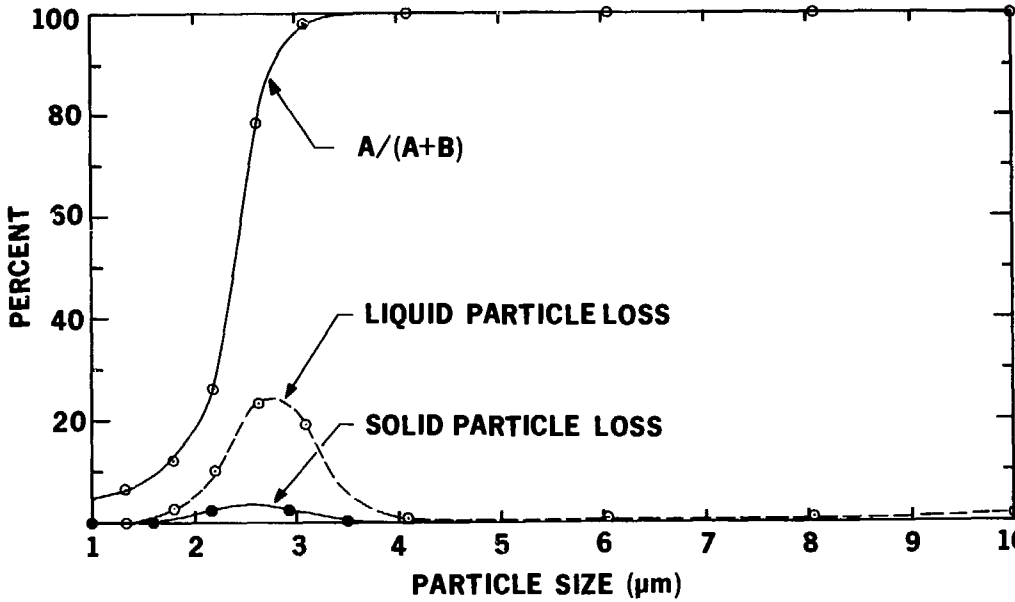

Figure 3. Cut point behavior and loss characteristics of the virtual impactor. The quantity A is the amount collected on the coarse filter; B the fine.

Table 1. Summary of Sites, Times, and Intervals for which Particulate Data are Available

SITE	DATES FOR WHICH DATA AVAILABLE	SAMPLING PERIODS
103	6-16-75 to 7-11-75	6 hrs.
	7-11-75 to 8-15-75	2 hrs.
	8-15-75 to 4-1-77	6 hrs.
105	6-16-75 to 7-11-75	6 hrs.
	7-11-75 to 8-16-75	2 hrs.
	8-16-75 to 4-1-77	6 hrs.
106	6-6-75 to 7-8-75	12 hrs.
	7-8-75 to 8-30-75	6 hrs.
	8-30-75 to 9-1-76	12 hrs.
108	6-14-75 to 7-10-75	12 hrs.
	7-10-75 to 8-16-75	6 hrs.
	8-16-75 to 7-30-76	12 hrs.
	7-30-76 to 9-3-76	6 hrs.
	9-3-76 to 4-1-77	12 hrs.
112	6-9-75 to 7-11-75	12 hrs.
	7-11-75 to 8-15-75	2 hrs.
	8-15-75 to 4-1-77	12 hrs.
115	6-20-75 to 7-7-75	12 hrs.
	7-7-75 to 8-16-75	6 hrs.
	8-16-75 to 7-26-76	12 hrs.
	7-26-76 to 9-1-76	6 hrs.
	9-1-76 to 4-1-77	12 hrs.
118	6-4-75 to 7-7-75	12 hrs.
	7-7-75 to 8-16-75	6 hrs.
	8-16-75 to 4-1-77	12 hrs.
120	6-23-75 to 7-9-75	12 hrs.
	7-9-75 to 8-22-75	6 hrs.
	8-22-75 to 3-31-77	12 hrs.
122	5-22-75 to 6-26-75	24 hrs.
	6-26-75 to 7-9-75	12 hrs.
	7-9-75 to 8-22-75	6 hrs.
	8-22-75 to 3-31-77	12 hrs.
124	5-23-75 to 6-27-75	24 hrs.
	6-27-75 to 7-10-75	12 hrs.
	7-10-75 to 8-17-75	6 hrs.
	8-17-75 to 8-29-75	12 hrs.
	8-29-75 to 9-7-75	6 hrs.
	9-7-75 to 8-26-76	12 hrs.

The temperature dependence of the flow control system results in a mass flow which is inversely proportional to the square root of the absolute temperature. Since short-term fluctuations in the pollutant level generally exceed effects due to the temperature variations, no corrections are currently applied. If one is calculating monthly averages from the data, it would be appropriate to apply a temperature correction for outside ambient variations.

The normal sampling schedule in St. Louis consisted of twelve-hour sample periods at all stations, except #103 and #105, where six-hour samples were standard. These latter stations routinely experienced higher particulate concentrations, which caused filter clogging in the longer sampling intervals. During an intensive study period during the summer of 1975, the schedule was modified to accommodate six-hour samples at most stations, with two-hour samples for stations #103, #105 and #112. Table 1 is a summary of the available data and sample intervals as recorded at each site.

The increased flow impedance, caused by particle loading on the membrane filter, was normally automatically compensated for by a reduction in the impedance of the flow control valve. In cases where the particle loading becomes excessive, the range of the flow control valve may be insufficient to compensate for the clogged filter. The full range of the flow control valve could accommodate an increase in impedance to twice the normal value. The sampler was programmed to automatically switch filters when this occurred. For the 1.2 μm membrane filter used in the study, fine particle mass loading of 200 mg/cm^2 or greater results in a 70% increase in the filter impedance which approaches the clogged condition.

The procedures followed in the sampling program were carefully controlled to ensure valid data. Individually numbered clean filters were loaded into separately numbered 36-sample cartridges at LBL. The sample identification number and the corresponding tare weight were recorded on magnetic tape at the time of the initial beta-gauge measurement. The samples were then shipped to St. Louis for exposure in the samplers. The location and time of sampling were recorded both on the cartridge labels and in a separate sampling log. This log also contained checklists for site visits and notes of any irregularities in the sample routine. The exposed filters were returned to LBL, together with the sampling information. Final weights were recorded and entered for each individual slide number. At the time of the X-ray fluorescence measurement, the data pertinent to the sampling conditions are entered into the computer system for subsequent data processing. The redundant sampling information allowed an accurate reconstruction of the sampling condition.

SECTION 3

MASS MEASUREMENTS

The total mass of particles collected in each size fraction is measured using an automated beta-particle attenuation method. An extensive discussion of the beta-gauge method as applied to aerosol samples can be found in Reference 5. The technique relies on the exponential dependence upon mass which the intensity of a continuous beta-particle spectrum exhibits when a variable thickness is placed between the radioactive beta source and a suitable detector.

Figure 4 is a schematic of the beta gauge showing a 300 μCi ^{147}Pm source, mounted in the upper vacuum chamber with a 2.5 cm diameter Si semiconductor in the lower chamber. The large area detector and large source to detector distance result in a uniform sensitivity over a large sample area. The measurement consists of inserting the membrane filter into the region between the source and detector and observing the change in total counting rate. When the system has been properly calibrated, the observed counting rate of pulses above a fixed threshold level can be related to the filter mass using the relationship:

$$I = I_0 \; e^{-\mu x} \qquad (1)$$

where I_0 and μ are the previously determined source intensity and mass absorption coefficient respectively. I is the observed counting rate and x is the mass per unit area of the filter.

Although the measurement is straightforward in principle, the use of beta attenuation in the present study is complicated by the high precision required. A typical measurement consists of determining the mass accumulated on a 4 mg/cm^2 filter to a precision of ± 10 μg/cm^2. This requires that each mass measurement be accurate to ~ 0.1%. The elapsed time between the measurements of the tare weight and the exposed weight might be several months, during which time it is likely that the measuring apparatus has been subject to deliberate or accidental changes. Furthermore, it is known that the exponential behavior of Equation 1 is not a fundamental characteristic of beta-particle attenuation, but is the fortuitous result of certain properties of the spectral shape of the beta particles. Small departures from ideal behavior are expected which can contribute to errors at the 0.1% level.

Our procedures employ frequent calibrations to eliminate many of the problems associated with system instability. A series of carefully weighed polycarbonate film standards which span the mass region of interest are measured with the beta gauge and the resulting count rates are determined.

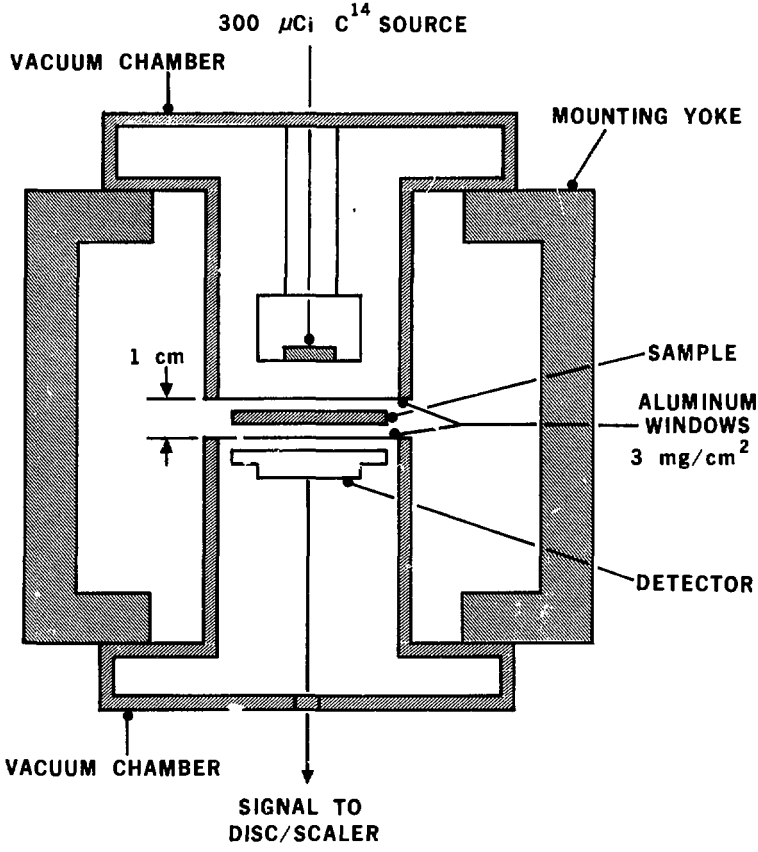

XBL 752-327

Figure 4. Cross section of beta gauge apparatus.

To achieve adequate statistical accuracies, counts are accumulated for 100-second intervals at a counting rate of ~ 10^5 counts per second. The resulting data of mass (mg/cm^2) versus counts per second are then fitted to Equation 1 by the least squares method. The resulting calculated values of I_0 and μ are then ed to calculate the unknown masses of the membrane filters. To ensure accurate fit to the data, the mass region spanned by the thin film standards is limited from 3 mg/cm^2 to 6 mg/cm^2. By performing a least square fit of the data over this interval to the function:

$$I = I_0 \; e^{-\mu x + \nu x^2} \qquad (2),$$

it is possible to show that the function approximates a pure exponential, since it is observed that $\nu x^2 \ll \mu x$. The deviations of gravimetric masses from the least square calculations are typically 3 $\mu g/cm^2$.

Additional corrections, which cannot be eliminated by frequent calibrations, are as follows:

RELATIVE HUMIDITY EFFECTS

Although the uniform, thin film standards used for calibration purposes are immune to changes in the ambient relative humidity, the cellulose ester filters used in the samplers are very susceptible to such variations. To permit corrections for this phenomenon, a series of 70 clean membrane filters were exposed to variable relative humidity and the effects on total mass were determined. Figure 5 shows the results. The fitted slope obtained from these data is 1.80 ± 0.02 $\mu g/cm^2$ increased mass for each percent change in relative humidity. The range of relative humidity encountered in our laboratory is 45 to 65%. The relative humidity is noted when filters are measured and the mass correction is applied to data at the time of computer analysis. No correction is made for humidity effects in the aerosol deposits, since over the limited range of relative humidities experienced in the laboratory, such a correction should be negligible compared to that for the substrate.

ATOMIC NUMBER DEPENDENCE

The rate of energy loss of electrons traversing a material of atomic number Z and mass number A is a complex combination of ionization, nuclear and electronic scattering and radiation losses. The actual rate of energy loss due to ionization decreases slightly with Z/A as Z is increased. However, the increase in scattering with increasing Z results in increased resultant path length. At low beta energies, the effect of scattering overcompensates the effect of having fewer electrons per gram in high Z material. This results in a dependence of the absorption on the average Z/A of the samples. This has been experimentally measured for a ^{147}Pm beta source by using a series of thin standards of various elements. A least squares fit to the experimental values gives:

$$\mu = \left[7.04 - 10.77 \frac{Z}{A}\right] \times 10^{-4} \; cm^2/\mu g \qquad (3)$$

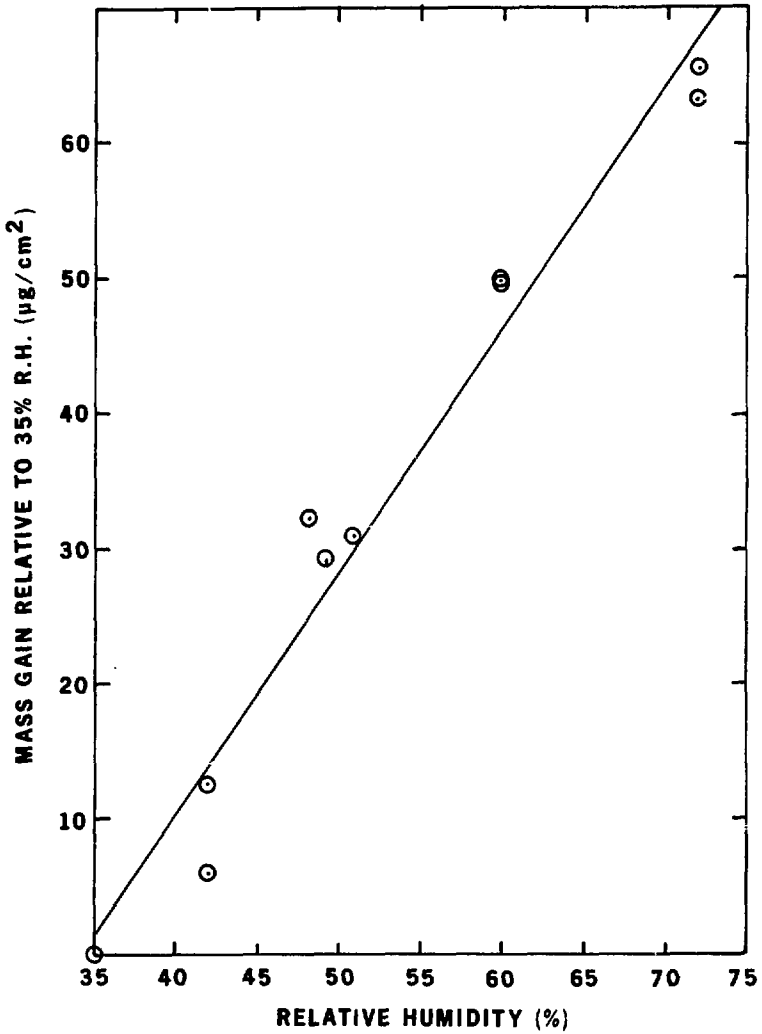

XBL 776-9209

Figure 5. Mass gain of 4 mg/cm^2 cellulose membrane as a function of % relative humidity.

Table 2. Atomic Number Dependence of Beta-Gauge Mass Attenuation Coefficient

MATERIAL	Z/A	μ ($10^{-4} cm^2/\mu g$)
$(CH_2)_n$	0.570	0.90
$(NH_4)_2 SO_4$	0.530	1.33
Polycarbonate	0.527	1.36
Carbon	0.500	1.66
Calcium	0.499	1.67
SiO_2	0.499	1.67
Al_2O_3	0.490	1.76
Fe_2O_3	0.476	1.91
Pb	0.396	2.78

This empirical formula can then be used to estimate the effect of aerosol composition on mass measurements by beta gauging. Table 2 shows the calculated absorption coefficients for some selected substances. The use of polycarbonate films as calibration standards causes the mass of heavier compounds, such as $(NH_4)_2 SO_4$ to be underestimated by about 3%; oxygen and most other elements from C to Ca will be overestimated by about 20%. Thus, the light hydrocarbons and the sulfates will have compensating effects with the more abundant elements below Ca. Since the heavier elements are usually present in trace quantities, they will contribute negligible errors. Even 10% by weight of Pb will introduce an error of about 5% in the accuracy of mass measurement.

FILTER POROSITY EFFECTS

As noted earlier, the calibration of the beta gauge is achieved through the use of carefully weighed polycarbonate film standards. Since the cellulose ester membrane filters consist of a microscopically nonhomogeneous and porous medium, there arises a discrepancy when their mass is determined using the calibration obtained from the continuous thin film standards. Since this discrepancy is constant for a given filter mass, it has no effect on the calculated mass difference before and after exposure. However, there are situations in which this discrepancy can become significant. We have observed that the magnitude of this effect depends on the amount of material which the beta particles have traversed before reaching the sample itself. For example, if the detector vacuum chamber window is changed from 2.40 mg/cm^2 to 4.00 mg/cm^2, an apparent change in measured mass of a 4 mg/cm^2 membrane filter of as much as 38 $\mu g/cm^2$ is observed when both systems were calibrated in the same manner.

A possible explanation for this phenomenon is that both the average energy and the angular distribution of the beta spectrum are changed by varying the amount of material traversed by electrons before reaching the sample. The change in angular distribution is brought about by multiple scattering and would be expected to affect the results more for a porous filter medium than for a uniform filter. Certain changes in the source-detector geometry might also be expected to produce similar effects upon the results.

In practice, the beta gauge apparatus is maintained in as constant a configuration as possible. Unavoidable changes, such as punctured vacuum windows do occur, however. A standard set of membrane filters is used to correct for the porosity effect when any beta gauge modifications occur. Once the effect has been calibrated, subsequent thin film standards are adequate until the next change in the system geometry occurs.

In spite of the necessity for such corrections, the beta-gauge technique still has the advantage of automatic operation for mass measurement in large-scale sampling programs. Using a computer controlled automatic sample change, the filters are individually counted for 30 seconds. The precision of this measurement is 4.3 $\mu g/cm^2$. After the difference between two such measurements is calculated and the various correction factors applied, the precision is estimated to be 10 $\mu g/cm^2$. This converts to an accuracy of aerosol mass determination of 12 $\mu g/m^3$ for a two-hour sample and 2 $\mu g/m^3$ for a twelve-hour sample. A total of 70,000 mass determinations have been performed in the course of the present study.

SECTION 4

X-RAY FLUORESCENCE MEASUREMENTS

The elemental composition of the particulate deposits were measured, using an energy dispersive X-ray spectrometer. Descriptions of this method have been reported extensively in the literature[8] and will be treated only briefly here. Among the advantages of energy dispersive XRF are its multiple element capability, high sensitivity for elements of interest, ease of automation and stability of calibration.

SENSITIVITY

The particular X-ray spectrometer employed is an LBL-constructed pulsed X-ray excitation system with computer controlled sample sequencing and analysis. The X-ray excitation is provided by a series of three secondary fluorescence targets, which are irradiated with the output of a pulsed X-ray tube. The advantages of the pulsed excitation are increased sensitivity for analysis and elimination of certain systematic artifacts which result from pulse pile-up in the conventional X-ray fluorescence spectrometer systems.[9] Using the three secondary targets, we routinely analyze 28 elements, although a larger number of elements could be monitored, if desired. A summary of the operating conditions are given in Table 3. Table 4 is a list of the elements measured and the associated sensitivity and minimum detectable limits for the analysis times normally employed. For a comparison of these detectabilities with other XRF methods, see Reference 10. Figure 6 is a plot taken from that paper, showing a comparison of the energy dispersive XRF method with typical elemental compositions for the atmospheric aerosol.* These data indicate that the method is sufficiently sensitive for the analysis of a wide variety of elements of interest in air particulate analysis.

PRECISION AND ACCURACY

The precision and accuracy of the XRF method are dependent upon many components in the system, each of which must be carefully controlled. This is particularly true in a large-scale, automated study where the system

*To convert from ng/cm^2 to ng/m^3, for the dichotomous samplers used in the study, the sampling rate is equivalent to 1 m^3/cm^2 in a two-hour period.

operates unattended for extended periods. For convenience, a discussion of errors can be separated according to the following areas: 1) excitation source instability, 2) reproducibility of sample geometry, 3) spectrometer stability, 4) errors in spectral analysis, and 5) systematic errors in calibration and data analysis. A discussion of each of these follows.

Table 3. Operating Conditions for Sampling and Analysis

Excitation:

- Pulsed X-ray tube, tungsten anode with secondary targets
- 85 watts average power

Detector:

- Lithium drifted silicon guard ring detector operated in anti-coincidence mode
- 30 mm^2 area, 195 eV resolution at 5.94 keV
- Maximum counting rate at 14,000 cp
- Pulsed optical feedback amplifier

Secondary targets, operating tube voltages, and analysis periods:

Ti,	50 kV,	1.6 minutes
Mo,	60 kV,	1.4 minutes
Sm,	75 kV,	2.6 minutes

Sampler characteristics:

Flow	--	50 ℓ/min.
Area	--	Approx. 7 cm^2
Cutpoint	--	2.4 μm

Excitation Source Stability

X-ray spectrometers are normally calibrated in terms of the yield of fluorescent X-rays obtained with a constant current flowing in the X-ray tube for some specified period of time. If the yield of excitation X-rays per electron at the anode is constant, and if the current and time are carefully measured, then the precision of the excitation is maintained.

In the pulsed X-ray system, the current and time measurements are replaced with an anode current integrator. Each analysis is then normalized to the calibration data according to the total charge which flowed in the X-ray tube during the measurement. This technique has distinct advantages over the conventional method, since corrections for pile-up and system dead time effects need not be considered.

Table 4. Sensitivity for Energy Dispersive X-Ray Fluorescence Analysis

ELEMENT	ATOMIC NUMBER	BACKGROUND[d] (counts/sec)	SENSITIVITY (counts/sec per μgm/cm^2)	MINIMUM DETECTABLE LIMIT (ngm/cm^2)
Al[a]	13	19.0	7.40	200
Si	14	19.2	25.3	58.9
P	15	21.6	48.0	32.9
S	16	52.3	83.8	29.4
Cl	17	95.8	125	26.6
K	19	53.2	272	9.14
Ca	20	86.4	411	7.7
Ti[b]	22	6.3	28.8	31.3
V	23	5.4	37.8	22.2
Cr	24	5.2	49.3	16.6
Mn	25	5.0	59.8	13.5
Fe	26	6.3	76.4	11.8
Ni	28	3.7	112	6.2
Cu	29	5.3	128	6.5
Zn	30	4.8	148	5.3
Ga	31	3.1	166	3.8
As	33	3.2	209	3.1
Se	34	2.9	234	2.6
Br	35	3.7	258	2.7
Rb	37	5.6	304	2.8
Sr	38	11.3	320	3.8
Hg	80	3.3	109	6.0
Pb	82	7.6	109	9.1
Cd[c]	48	2.8	75.5	5.9
Sn	50	5.0	75.7	7.8
Sb	51	5.3	74.6	8.1
Ba	56	52.4	62.1	31

a) These elements were analyzed for 93.6 seconds, using a Ti secondary target.

b) These elements were analyzed for 83.4 seconds, using a Mo secondary target.

c) These elements were analyzed for 153 seconds, using a Sm secondary target.

d) The background was obtained using a blank membrane filter.

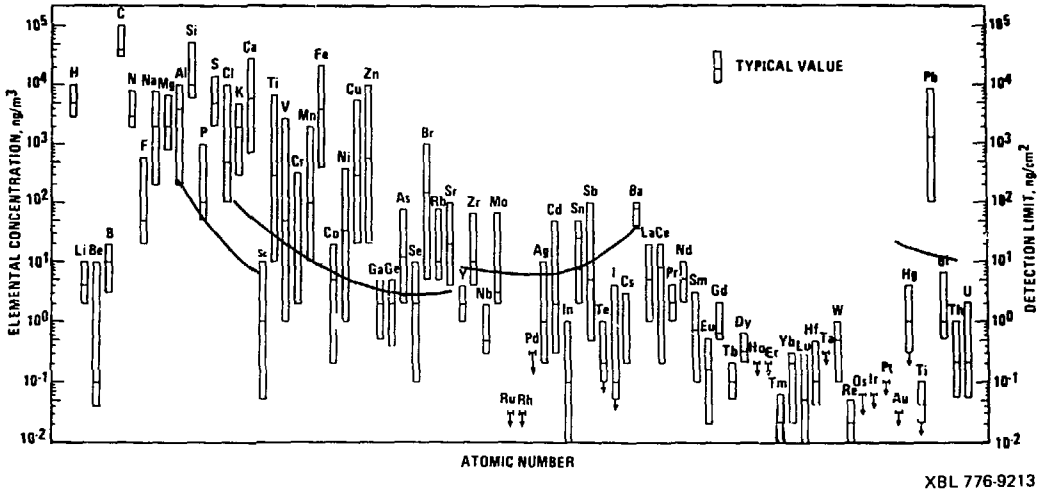

Figure 6. Minimum detectable limit for X-ray fluorescence analysis compared with average aerosol concentration ranges.

The reproducibility of the charge integrator was checked by observing the linearity of the X-ray yield with the integrated charge. A more stringent test involved the measurement of the stability of the calibration under varying count rate conditions. A thin-film standard of Fe was first counted for a fixed amount of collected anode charge and the Kα intensity recorded. A thick scatterer was then placed behind the Fe standard and the measurement repeated. The effect of the scatterer was to reduce the average direct current in the tube by a factor of 20. However, the system compensated by increasing the counting time, resulting in the same total integrated charge. The extent to which the Fe Kα intensity remained unchanged is a measure of the accuracy of the current integrator method. A 3% agreement was observed.

Variations in the X-ray yield per unit charge at the anode are caused principally by the energy dependence of the X-ray production cross sections in the X-ray tube and secondary fluorescence targets. This dependence can be measured by observing the yield of fluorescent X-rays from a standard sample as the tube anode voltage is changed. Figure 7 is a series of plots, showing the measured voltage dependence for each of the three secondary fluorescers. Since the X-ray tube voltage is regulated to be stable to < 1%, the calculated slopes at the operating voltages indicate output variations less than 1.2, 2.8 and 3.3% for F1, F2 and F3 respectively.

Other possible sensitivity variations due to changes in the tube-fluorescer geometry have been checked and found negligible under normal operating conditions.

Reproducibility of Sample Geometry

Variations in the system sensitivity could be caused by the fact that the excitation and detection efficiencies are functions of the positions of the sample in the detector collimator field of view. Figure 8 is a view of the X-ray tube secondary target detector geometry. The sample is introduced horizontally into this region by means of an automatic sample changer. A scan of the sensitive area for the case of the Mo secondary fluorescer is shown in Figure 9. These curves were obtained by moving a point Cu specimen horizontally across the region where the membrane filters are normally placed. Curve a) is a scan of the axis, perpendicular to the view of Figure 8. Curve b) is a scan from right to left in the same view. The detector collimator opening was deliberately chosen to restrict this sensitive region to an area much less than the typical 30 mm diameter deposit on the filter. For this reason, the fluorescence intensity is not sensitive to small displacements of the sample in the horizontal plane, providing that the sample is uniform over the exposed area.

Vertical displacement of the sample in the sensitive region can potentially have a larger effect on the observed intensity. The membrane filters are not always perfectly flat, resulting in a variation in vertical distance from point to point across the filter. We have measured the change in

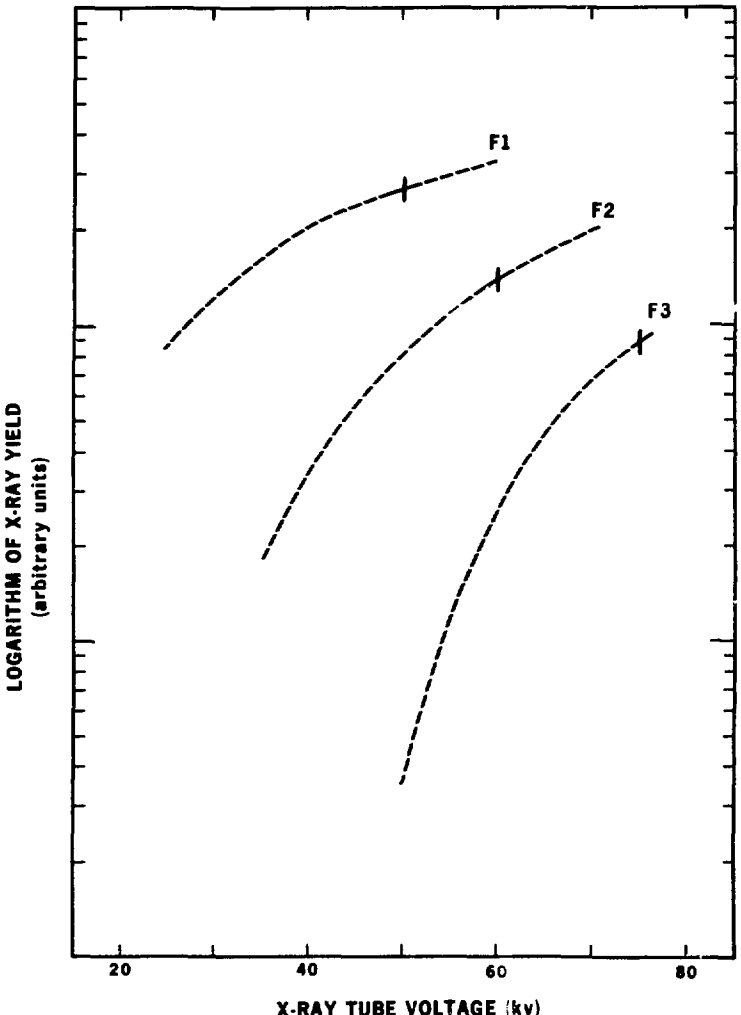

Figure 7. Voltage dependence of X-ray yield in X-ray fluorescence unit. Vertical line on curve represents normal operating voltage.

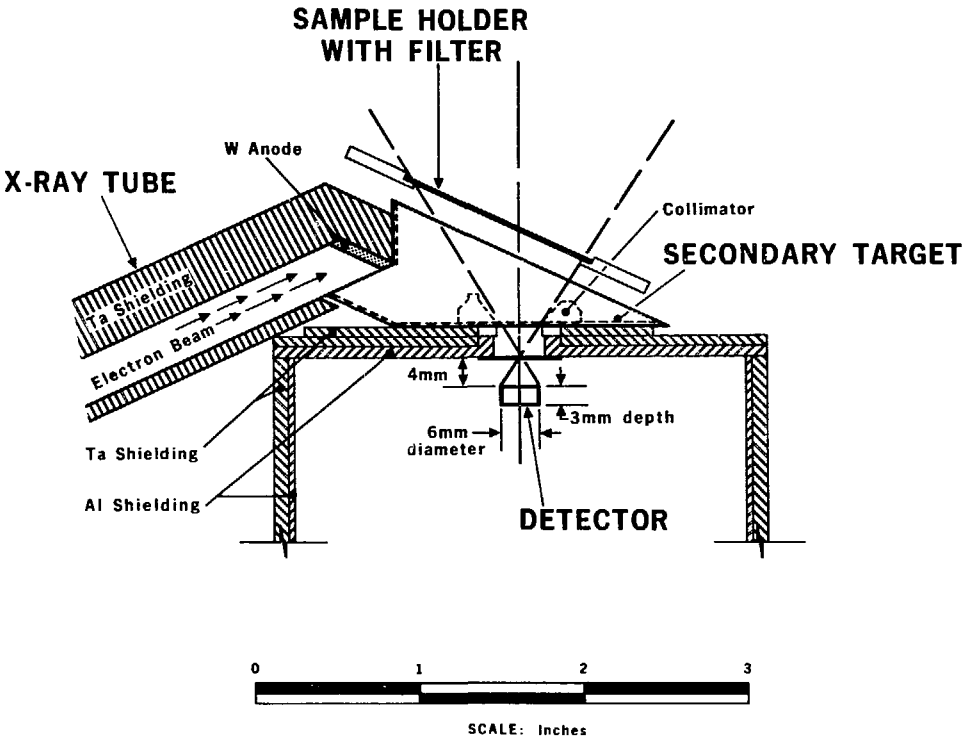

XBL 731-102

Figure 8. Cross section of secondary fluorescence geometry.

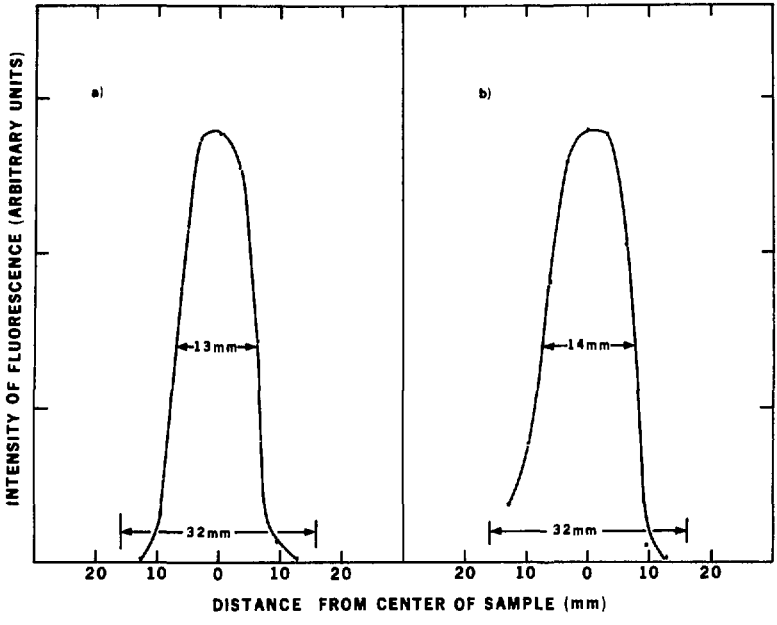

Figure 9. Scans of sensitive region of X-ray fluorescence unit.

fluorescence output for a uniform thin sample as a function of the vertical displacement of the sample and a change of 16% was observed for a 1 mm displacement. Assuming a maximum departure from flatness of 0.5 mm, then the output variation would be less than 8%. In practice, the observed error is much less than this.

Spectrometer Stability

The characteristics of the Si(Li) semiconductor spectrometer system which can potentially affect the results are changes in the absolute efficiency, peak-to-background ratios, system resulution, and peak locations. In a typical spectrometer system, the absolute efficiency and peak-to-background ratios are easily stable within the limits of concern for the present analytical applications. Although some variations in these parameters have been observed in the past, they were attributed to artifacts in the system design which have been eliminated.

The energy resolution of the system is also quite stable if problems due to local electrical noise are eliminated. To reduce these problems, our system is operated from a regulated ac source and care is taken to eliminate local sources of noise, such as drill motors, etc. Frequent checks of the system resolution are made; to date, no significant changes have been noted.

Stability of the peak location in the multichannel spectrum is affected by long-term drifts in the amplifier baseline and gain. These are normally associated with variations in the ambient temperature. In the present case, the temperature is maintained reasonably constant by using a room air conditioner. Nevertheless, it is difficult to maintain stability below the limits of observation. For a peak with 200 eV resolution at 20 keV, a stability of ± 2 eV represents changes in amplifier gain of one (1) part in 10^4. For this reason, the gain and baseline are checked weekly and fine adjustments made where necessary to maintain them at their reference value. The corrections are made by calculating the centroid of the Ar $K\alpha$ (2.95 keV) and In $K\alpha$ (24.2 keV) peaks and adjusting controls to return these peaks to their reference position. Root mean square deviations of these centroids, which have been observed over several one-week periods, are ± 5.3 eV for the 2.95 keV line and ± 4.8 eV for the 24.2 keV line.

The effect of these variations on the accuracy of the complete analysis is difficult to assess. Changes in peak locations are partially compensated for in the spectral analysis program. However, such shifts introduce errors into the analysis of small peaks which are close to very intense lines, since residuals are left after stripping the large peaks from the spectra. Since there is no systematic way to predict such circumstances, the best check of such errors is in the repeated analysis of standards which replicate typical air particulate samples.

Errors in Spectral Analysis

Energy-dispersive X-ray fluorescence analysis requires data reduction procedures to convert the multi-element spectral data into peak intensities of the individual elements. The problems of the subtraction of background and possible overlap of peaks from different elements must be handled by the computer algorithms.

There are many methods of analyzing spectral data.[11,12] All are capable of extracting peak intensities for clearly resolved major constituents with an accuracy limited only by statistical errors in the peak and background integrals. However, the intensities of smaller peaks which overlap larger peaks are much more difficult to extract, since they can be affected by small shifts in peak position and by peak and background shapes. Furthermore, specification of the error margins in these cases is very difficult. The present discussion focuses on the specific method of spectral analysis used by us, and avoids discussion of sources of error beyond the normal statistical considerations. The best practical estimate of total errors is obtained by determining the reproducibility of a large number of measurements made on a few samples whose compositions are typical of those encountered in normal environmental samples.

The on-line spectral analysis program used in the present study is a straightforward stripping procedure illustrated in Figure 10. A background spectrum produced by a blank filter and standard spectra for all individual elements are stored in the computer memory. The unknown spectrum is then reduced by subtracting the stored background, which is normalized appropriately by comparison over a selected region and then by sequentially stripping out the contributions to the spectrum due each element using the stored spectral line shapes for the elements. The line shapes subtracted involve an extended region of interest including K_α and K_β and more extensive regions in the case of L X-ray spectra. The amount of each standard elemental spectrum subtracted from the unknown spectrum is chosen to best fit the intensity of the unknown X-ray. Peak areas are then converted to concentrations in ng/cm^2 by applying the appropriate excitation and detector efficiency factors. These calculations are described in greater detail below.

With the exception of a few cases, most importantly the Pb L overlap with the As K_α X-rays, the method of spectral analysis works particularly well for air particulate samples, because a membrane filter consists of a thin homogeneous substrate on which the elements to be measured are deposited. These properties of the substrate are almost constant from one sample to the next and are identical, essentially, to those of the blank filter whose spectrum is stored as a background standard. Since the samples are thin, absorption effects will not alter the spectral response of the system to a given set of characteristic X-rays.

This method neglects the effect of an X-ray from one element overlapping that of another. This effect can be handled after the spectral analysis,

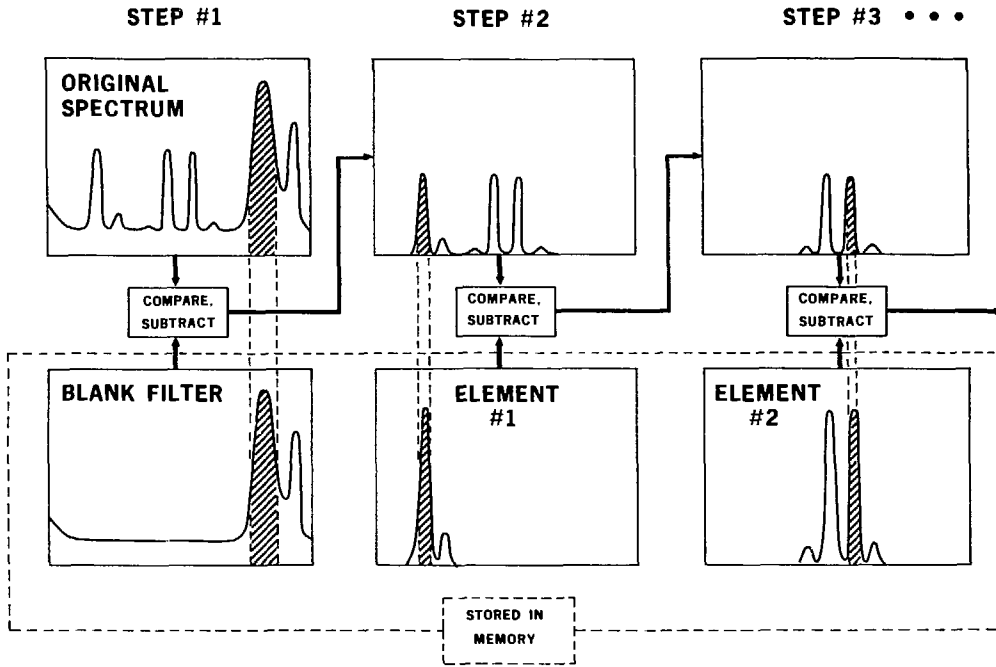

XBL 731-86

Figure 10. Diagram of spectrum stripping procedure.

however, by using a simple formula which assumes that the intensity of a given element can be expressed as:

$$I_i = I_i - \Sigma_j C_{ij} I_j \quad (4)$$

when C_{ij} is a measure of the interference of element j with the principal line of element i. In sophisticated analysis programs, these expressions can be iterated to achieve self-consistency. However, since the number of overlapping lines in a typical environmental sample spectrum is small, a simple one-step calculation involving experimental measured C_{ij} is normally adequate.

The C_{ij} is determined using a thin standard containing a known amount of element j and measuring the contribution of this standard to the intensity of the line due to element i. The thin film standards are selected so as to ensure negligible absorption of the very low energy X-rays.

The most sensitive indicator of the effectiveness of this spectral analysis method is observation of the residual intensities left in the pulse-height spectrum after the stripping procedure has been completed. Ideally, the remaining counts in the multichannel spectrum should be evenly distributed about zero, with deviations reflecting only the combined statistical uncertainties of the original sample and background spectra. Any structure or residual intensity in the form of peaks above statistical background must be regarded as an artifact resulting from imcomplete stripping of the X-ray lines or from the effect of shifts in the unknown spectrum relative to the standards. Over several years of operating experience in the present study, it has been observed that if the system is properly calibrated and maintained in a stable configuration, the residual spectrum has always been free from such structure. However, periodic checks are made to ensure that the spectral analysis is operating properly.

CALIBRATION ACCURACY

The errors we have discussed so far are primarily those affecting the precision of measurement, i.e., the reproducibility over extended periods of time and under varying analytical conditions. The absolute accuracy of the X-ray fluorescence analysis is determined almost entirely by the calibration procedures.

In its simplest form, the determination of elemental concentrations using a X-ray fluorescence spectrometer consists of relating the peak intensities observed in a spectrum to the concentration of the various elements present on the filter. We have:

$$C_i = N F_i I_i / A_i \quad (5)$$

where C_i is the concentration in ng/cm^2, I_i is the observed counting rate for element i, F_i is the calibration factor appropriate for a thin specimen of element i (related to the sensitivity of Table 4 as $F_i = 1/Si$), A_i is a factor which corrects the results for attenuation of the

fluorescent X-ray as it leaves the sample and N is a normalization factor which scales the result according to the analysis time or integrated current.

The normal calibration procedure uses thin, uniform standards which closely replicate the geometry of the air particulate filters. These standards have been calibrated either directly by gravimetric measurement or by reference to another standard. The term "thin" implies that $A_i = 1$ for these standards.

For the lower energy fluorescence X-rays produced in a filter deposit, absorption effects can occur either because of the location of the individual particles within the filter matrix or because of attenuation of the X-rays arising within an individual particle. Corrections for matrix and particle size effects are contained in the factor A_i, and are applied during the later stages of data analysis. The overall accuracy of the measurement then includes uncertainties in the thin standard calibration and those associated with the absorption corrections (see Table 11).

Thin Film Calibration

The use of thin film calibration has been discussed extensively in the literature.[13,14] The procedure consists of measuring X-ray yields for elemental standards distributed across the range of atomic numbers of interest and then interpolating for elements not directly measured. The validity of the interpolation procedure results from the smooth behaviour of the X-ray cross sections as a function of the atomic number of elements.

In the present calibration, a series of thin film Cu standards were used as the primary calibration standard. These standards consisted of an evaporated layer of Cu on mylar substrate and were obtained from Micro-matter, Inc. These standards have been extensively cross-checked with other gravimetric standards, using several independent X-ray fluorescence measurements. These standards are accurate to better than 2%.

The relative excitation efficiencies for the elements were obtained using thin film standards prepared by depositing an aerosol generated from a carefully prepared solution in which the relative concentrations of the elements was previously known. Where possible, the ratio of elements was established by the stoichiometry of the chemical compound. In other cases, solutions containing individual elements are mixed in known ratios according to a method described by Giauque.[15] The principal selection criteria were compounds which did not react in solution and whose characteristic X-rays produced no overlapping lines in the spectra. Table 5 is a summary of the elements and compounds which were used. The accuracy of the ratios obtained by this method are estimated to be less than 1%.

Because of the importance of sulfur in this program, exceptional care was taken in its calibration. Thin film standards were prepared by collecting an aerosol deposition for particles of 0.3 μm diameter in order to eliminate absorption effects. The compounds used for the deposition were

$CuSO_4$, K_2SO_4 and $K_2Cr_2O_7$. The calibrations were then referred to the Cu standard through the following three paths: Cu→S, Cu→K→S and Cu→Cr→K→S. The agreement between these three independent determinations of the sulfur calibration was within 3%.

The calibrations for the very light element Al and Si are complicated by the strong attenuation of the low-energy X-rays. For these cases, thin (~ 100 μg/cm) evaporated films are used for the direct calibrations. The inherent inaccuracies due to the attenuation effects experienced by these elements are reflected in the increased analytical error in the determinations.

Table 5. Calibration Solutions for Thin Aerosol Deposited Standards

Element	K	Cu	Cr	Mn	Fe	Ni	Cu	Zn	Sr	Rb	Ag	In	Ba	Pb
Compound	$K_2Cr_2O_7$	$CuCO_3$	$K_2Cr_2O_7$	Mn	Fe	Ni	Cu	Zn	$SrCO_3$	RbCl	$AgNO_3$	In	$BaCO_3$	Pb
Solvent	HNO_3	HNO_3	HNO_3	HNO_3	HCl/ HNO_3	HNO_3	HNO_3	HNO_3	HNO_3	H_2O	H_2O	HNO_3	HNO_3	HNO_3
Elements with which combined	Cu	Cu	Cu	Cu Zn Pb Sr	Cu	Mn	K Cr Fe Ca Mn Ba	Mn	Mn In	In	In	Sr Ag Ba Pb Rb Sr	In	In Mn

Table 6 contains a list of the calibration factors and their associated errors as determined by the procedures described below. The adopted values are obtained by demanding a smooth curve fit through the measured data points. These calibration factors are the reciprocals of the sensitivities listed in Table 4 and are normalized to unit charge collected in the X-ray tube instead of unit time of analysis.

Absorption Effects

Absorption of fluorescence X-rays within the sample can occur in either of the two ways illustrated in Figure 11. The diagram of 11a) illustrates the matrix attenuation which an X-ray produced at the depth x experiences. The incoming beam I_0 is attenuated by $e^{-\mu_0 x}$ where μ_0 is the coefficient for energy E_i.

The complete matrix absorption correction for particles collected on a filter of thickness d is calculated by integrating the absorption expressions over the thickness of the filter assuming a particle density distribution p(x). If we assume a surface deposition, then the absorption correction $A_i = 1$. If we assume a uniform deposition of p(x) = constant, then it can be shown that:

$$A_i = \frac{1 - e^{-(\mu_0 + \mu_i)pd}}{(\mu_0 + \mu_i)pd} \qquad (6)$$

Typical estimates of the factor A_i assuming a uniform deposition of particulates within the filter are 0.87 for Ca, 0.67 for S, and 0.30 for Al $K\alpha$ X-rays. Since observed particle deposition profiles indicate that a surface deposition model is a close approximation to real samples, the values obtained from equation (6) should be considered as upper limits or possible matrix absorption corrections.

Loo, et al[15] have studied the effect of surface deposition and its effect on the analysis of sulfur in great detail. They have found that surface deposition normally occurs except in circumstances in which a high relative humidity of ambient air occurs in combination with high particulate concentrations. Under these conditions, the sulfur-containing particles tend to migrate into the filter and the deposit can approach a uniform depth deposition. A method of measuring A_i has been employed which determines the apparent X-ray intensity from both sides of the filter. The ratios of these two values is then related to the particle deposition within the filter. In the course of the study, it was observed that certain filters exhibited ratios of X-ray intensities which were close to unity, indicating considerable penetration of particles into the matrix. In order to correct the light element concentrations for this effect, all of the fine particle filters were remeasured on the reverse side. The front-to-back ratio of

Table 6. Summary of Calibration Measurements

Element	Measured Calibration Factor[a)]	Adopted Value
Al		0.70
Si	2.4 ± 0.5*	2.39
P		4.54
S	7.84 ± 0.14	7.92
Cl		11.85
K		25.64
Ca	38.8 ± 0.6	38.8
Ti		2.38
V		3.12
Cr	4.07 ± 0.07	4.07
Mn	4.94 ± 0.08	4.94
Fe	6.31 ± 0.1	6.31
Ni	9.23 ± 0.15	9.23
Cu	10.55 ± 0.19*	10.55
Zn	12.19 ± 0.16	12.19
Ga		13.75
As		17.3
Se		19.3
Br		21.3
Rb	25.1 ± 0.20	25.1
Sr	26.4	26.4
Hg		9.00
Pb	8.98 ± 0.16	9.00
Cd	5.64 ± 0.14	5.62
Sn	5.91 ± 0.6*	5.63
Sb		5.55
Ba	4.62 ± 0.11	4.62

a) Units are in cts/sec per $\mu g/cm^2$ for a constant amount of charge collected at the X-ray tube anodes.

Errors are based on root mean square deviation of several independent standards, except those marked (*) which were evaporated standards.

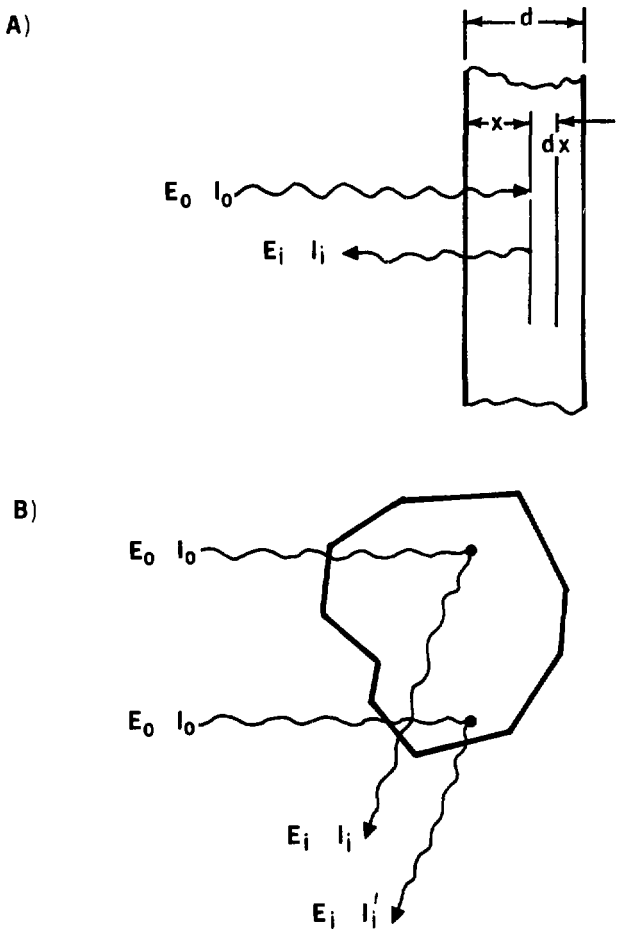

XBL 806-10381

Figure 11. Illustration showing matrix absorption effects (A) and large particle attenuation (B).

sulfur concentration was then used to calculate a filter penetration correction using the model developed in Reference 16.

The particle size effects are illustrated in Figure 11b). Here the intensity of I_i and I_i' are different due to the different path lengths in the particles. Again, the magnitude for this effect is dependent upon the energy of the fluorescence X-ray and is worse for the light elements.

The estimation of the attenuation A_i due to this effect requires the assumption of a specific model of particle compositon and morphology. Fortunately, the use of the dichotomous sampler isolates those particles less than 2 μm diameter where such effects are minimal. The large particle attenuation, however, cannot be ignored.

We use the value calculated by Dzubay and Nelson[16] which assume uniform spheres of composition approximately that of typical aerosol particulates. Table 7 is a tabulation of those corrections for two size ranges. It should be noted that the fine particles S determinations are not significantly affected by this correction.

REPRODUCIBILITY OF RESULTS

The reproducibility of the aerosol samples has been checked by collecting side-by-side samples at LBL, using three automatic dichotomous samplers. Two of the units had been in continuous operation at St. Louis for two years prior to the test, the third had remained at LBL. None of the flow controllers had been adjusted since their original checkout following initial fabrication.

Table 8 is a summary of results obtained from three separate sampling intervals as measured by the XRF analysis of the deposited particulates. The root mean square (RMS) deviation for the coarse particle fraction is approximately 5%, whereas the fine particles reproduce to less than 1.5%. This result is consistent with the greater variability in coarse particle collection efficiency.

The precision of the XRF analysis was checked by the repeated analysis of the same filters over an extended period of time. In addition to checking the stability of the total spectrometer system, this test will also give some indication of the accuracy and stability of the spectral analysis program. Table 9 is a list of average concentrations and RMS deviations obtained from ten successive measurements of the same filter carried out periodically over a three-month period. The reproducibility of the major elements indicates a stability of approximately ± 1% over this interval as indicated by the error in the major elements. The small, relative error for minor constituents, such as Mn and Ti, give some indications of the reproducibility of the computer spectral analysis. The results are particularly impressive when we emphasize that these measurements were performed periodically during an interval when the system was continually analyzing 500—1000 samples per week automatically, and no special attention was devoted to these particular analyses.

Table 7. Particle Size Attenuation Corrections for the Light Elements. (Adapted from Reference 14). F1 and F2 refer to the secondary fluorescence targets Ti amd Mo respectively.

Element	Fine Particle Correction		Coarse Particle Correction	
	F1	F2	F1	F2
Al	0.91 ± 0.09	1.0 ± 0.0	0.41 ± 0.12	
Si	0.93 ± 0.07	1.0 ± 0.0	0.48 ± 0.15	
P	0.95 ± 0.05	1.0 ± 0.0	0.58 ± 0.24	
S	0.97 ± 0.03	1.0 ± 0.0	0.64 ± 0.22	
Cl	0.98 ± 0.02	1.0 ± 0.0	0.70 ± 0.20	
K	0.99 ± 0.01	1.0 ± 0.0	0.78 ± 0.15	0.83 ± 0.13
Ca	0.99 ± 0.01	1.0 ± 0.0	0.81 ± 0.13	0.86 ± 0.10
Ti				0.87 ± 0.10
V				0.90 ± 0.08
Cr				0.92 ± 0.07
Mn				0.93 ± 0.06
Fe				0.94 ± 0.05
Ni				0.96 ± 0.03
Cu				0.94 ± 0.06
Zn				0.95 ± 0.05

Table 8. Reproducibility of Air Samplers Measured by Side-By-Side Sampling

Element	Particle Size	Mean Concentration (ng/m^3)	Average Deviations (%)
S	Fine Coarse	1218 250	0.5 a) 2.5
Pb	Fine Coarse	1154 369	1.2 a) 2.9
Fe	Fine Coarse	208 1622	2.0 4.6 b)

a) Since S and Pb are predominantly in the small particle fraction, these errors should be considered representative of the precision for collection of fine particles.

b) This error should be the precision for the collection of coarse particles.

Table 9. Root Mean Square Deviations of Analyses of Identical Samples Over a Three-Month Period

Element	Average Concentration (ng/cm^2)	Deviation (ng/cm^2)	Deviation
Al	740	33.0	4.5
Si	2397	40.0	1.7
P	217	15.0	6.9
S	11693	189.0	1.6
Cl	298	9.2	3.1
K	515	7.7	1.5
Ca	3959	55.0	1.4
Ti	123	18.0	14.6
Mn	48.1	5.5	1.1
Fe	1930	18.0	0.9
Cu	123	5.9	4.8
Zn	519	29.0	0.6
Br	126	2.0	1.6
Pb	653	5.5	0.9
Sr	12.9	1.1	8.5
Cd	24.8	1.6	6.4
Sn	34.8	2.1	6.0
Sb	6.8	2.0	29.0
Ba	102	5.0	4.9

As noted in preceding sections, the accuracy of the measurement depends primarily on the accuracy of the thin film calibrations for mass and elemental concentrations and secondarily on the accuracy to which the various absorption and inter-element corrections for XRF analysis are known. The accuracy of the thin film standard is specified by reference to gravimetric methods. These standards have been further validated by an intercomparison study and agreed with the mean of results from three laboratories to better than 2%.[17]

The accuracy of the complete analysis is verified by intercomparison of the analyses with other laboratories and methods. This is currently being performed as validated results from other RAPS measurements become available. In the interim, a detailed comparison of results obtained by Robert Giauque of LBL uses independent XRF measurements of the same samples. As can be seen in Table 10, this agreement is to within 5% for major elements.

It should also be pointed out that extensive intercomparison studies involving our laboratory and others have been carried out in order to validate the XRF method. The studies have been published and in general, the agreement is excellent.[18, 19]

Table 10. Comparison of our Analyses with Independent XRF Measurements by R. Giauque.

Element	Sample 1		Sample 2		Sample 3		Sample 4	
	R. Giauque	Ours	R. Giauque	Ours	R. Giauque	Ours	R. Giauque	Ours
S	0	0	20400 ± 400	22289 ± 440	30600 ± 610	33700 ± 670	14100 ± 280	15169 ± 303
K	723 ± 132	684 ± 3	343 ± 133	577 ± 6	739 ± 136	770 ± 7	1264 ± 141	1517 ± 10
Ca	524 ± 53	839 ± 18	320 ± 58	451 ± 58	698 ± 62	820 ± 56	1853 ± 73	2136 ± 20
Ti	91 ± 21	166 ± 9	- 124 ± 24	0	- 78 ± 25	79 ± 9	- 95 ± 25	43 ± 21
V	31 ± 17	41 ± 7	50 ± 19	19 ± 5	29 ± 19	20 ± 7	70 ± 20	76 ± 8
Cr	33 ± 12	41 ± 1	- 24 ± 15	0	- 27 ± 15	8 ± 6	- 27 ± 15	6 ± 4
Mn	87 ± 11	122 ± 8	27 ± 11	37 ± 3	49 ± 12	76 ± 6	173 ± 14	195 ± 12
Fe	1225 ± 17	1327 ± 11	689 ± 14	716 ± 9	1185 ± 17	1190 ± 5	3980 ± 29	3975 ± 20
Ni	15 ± 3	21 ± 1	21 ± 4	16 ± 1	15 ± 4	18 ± 3	33 ± 5	47 ± 2
Cu	46 ± 4	68 ± 2	50 ± 5	50 ± 1	79 ± 5	63 ± 7	87 ± 6	121 ± 8
Zn	155 ± 5	173 ± 3	306 ± 6	294 ± 6	499 ± 8	482 ± 8	3634 ± 19	3534 ± 14
Ga	19 ± 5	0	7 ± 4	0	7 ± 4	0	0 ± 4	0
As	63 ± 16	21 ± 10	14 ± 9	0	43 ± 12	0	28 ± 4	9 ± 6
Se	53 ± 3	55 ± 1	17 ± 2	15 ± 3	24 ± 3	24 ± 2	8 ± 2	8 ± 2
Br	446 ± 6	520 ± 5	194 ± 4	212 ± 5	301 ± 5	318 ± 6	174 ± 4	185 ± 3
Rb	0 ± 3	0	2 ± 3	0	- 1 ± 3	0	7 ± 3	8 ± 1
Sr	15 ± 3	14 ± 1	2 ± 3	3 ± 3	11 ± 4	5 ± 1	10 ± 3	7 ± 2
Hg	0 ± 6	5 ± 2	6 ± 5	6 ± 3	17 ± 6	19 ± 3	0 ± 5	5 ± 5
Pb	3050 ± 23	3221 ± 22	991 ± 15	962 ± 4	1759 ± 18	1751 ± 32	1012 ± 15	992 ± 9

Values listed are in ng/cm^2. Errors are 1 σ for counting statistics only.
Ti, V, Cr, Mn values uncorrected for Ba L X-rays.

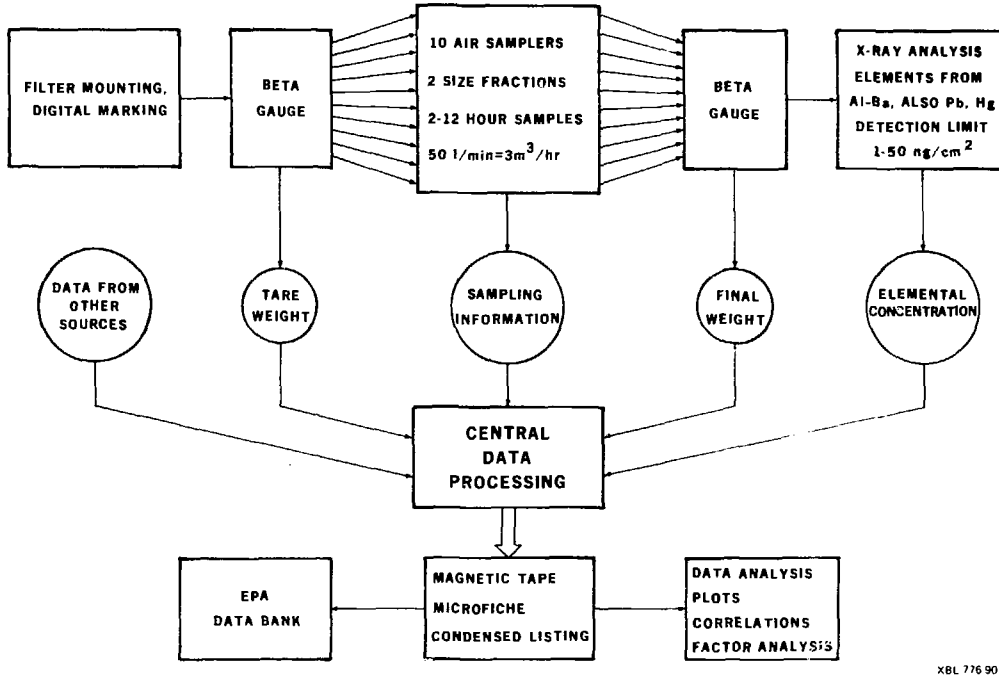

Figure 12. Flow chart showing the overview of sampling, analysis and data merging.

SECTION 5

DATA HANDLING

A considerable portion of the effort involved in the program was concerned with data storage and analysis. The results of mass and elemental composition for the 30,000 samples had to be sorted, processed and stored in some reliable and, hopefully, intelligible fashion. A complete flow chart for the operation is shown in Figure 12.

The data handling began with the tare weights as measured by the beta gauge prior to the field sampling. These beta experimental tapes contained calibration information and filter masses and were listed according to sample number only. On returning from the field, a second measurement of mass was made and a second data tape generated. This data was also catalogued according to sample number, although the sequence of sample numbers was not the same as in the tare weights. These two data tapes were then merged into a single data tape in which the initial and final masses were merged and stored according to sample number.

The samples were then sent for XRF analysis. At this time, the sampling information was entered. The sampling station, time of sample, sample interval and other information concerning the details of the XRF analysis were written on the magnetic tape output along with the results of that analysis. The information is now available to order the samples according to time and place.

The data tapes from both the beta gauge and XRF analyses were then written into a file which is approximately one-half the storage capacity of a 40-million-word disk file. The data were ordered according to sample number. A combination sorting and data processing program then merged the data sets and generated the final output. In order to apply the necessary corrections for each sample, it was necessary to have available not only the mass and elemental concentrations for each sample but also the corresponding data for the matching size fractions. For this reason, it was necessary that the sorting and merging of data be done with the largest possible data file available.

Table 11 is a summary of the data reduction procedures which were applied to the data. These include particle size corrections for all elements where appropriate, a combined layer and filter penetration correction, interelement interference correction, and the correction for cross contamination of fine and large particle size fractions. The final data were then converted to ng/m^3 and written on the second half of the large disk file. At this point, the data were ordered according to station number and

sequential time interval. Then the data were written onto magnetic tape and sent to the RAPS data bank at the Division of Meteorology, Environmental Sciences Research Laboratory, Environmental Protection Agency, Research Triangle Park, North Carolina.

The data were copied at EPA onto a single nine-track, 1600 bit density tape having a format described in Table 12. The status bytes are used as a quick summary of available data and are useful when preparing to merge the data sets. They are interpreted as a six-digit word with each digit corresponding to a particular measurement. These interpretations are given in Table 13.

As of February 1980, work on the data sets and corresponding output tapes has been completed. The data have been submitted to the EPA and are available from the National Technical Information Service (NTIS) as a part of the St. Louis RAPS study.

Table 11. Sequence of Calculations Performed on Original X-Ray Fluorescence Results.

The subscript i denotes a particular element; the other subscript is F or C corresponding to fine or coarse particulate fraction.

1) Original results read from X-ray fluorescence analysis output:

$$C_{iF} \pm \Delta C_{iF}$$

$$C_{iC} \pm \Delta C_{iC}$$

2) Layer correction, particle size correction and coarse/fine impactor cross-contamination correction:

$A_i \cong$ layer correction for fine fraction. It is derived from equation 6 using the measured mass of deposit and assuming an absorption typical for SO_4 ions.

$B_{iFC} \cong$ particle size correction, obtained from Table 7.

$$C_{iF}' = C_{iF}/A_i \; B_{iF} \; (0.95)$$

$$C_{iC}' = (C_{iC} - 0.0526 \; C_{iF})/B_{iC}$$

3) Inter-element interference correction. The constants D_{ik} are obtained from thin film measurements and represent the contribution of element k to the measured intensity of element i.

$$C_i'' = C_i' - \sum_{k \neq j} D_{ik} \; C_k$$

In the case of the lead/arsenic correction, the error is increased but no change in concentration is calculated since the spectral stripping program does this explicitly.

4) Convert results to concentration per unit sampling volume.

$F \cong$ flow per unit area of the particular sampler.

$T \cong$ sampling interval.

$$C_i^V = C_i''/(F) \; (T)$$

Table 11 continued.

5) Apply filter penetration correction to fine particle sulfur measurements. The model assumes surface deposition together with an exponential distribution in the filter matrix as discussed in reference 10. The substrate mass is obtained from the beta-gauge tape weight measurements.

6) Error calculations are performed explicitly using the normal quadrature addition formula:

$$\sigma^2 (C') = \sigma^2 (C) \sum_i \frac{\delta C'}{\delta X_i} \sigma^2 (X_i)$$

where $_i$ represent the variables used in the calculations. In cases where the associated errors are small such as in the sample rate or interval, they are neglected.

Table 12. RAPS Dichotomous Sampler Data

Logical Record Length is 444 Characters
Block Size is 4440 Characters

Character Position	Field Identification	Fortran Format
1-3	RAMS SITE ID	I3
4-7	YEAR	I4
8-10	JULIAN DAY	I3
11-14	SAMPLE START TIME	I4
15-18	SAMPLE DURATION	I4
19	FILTER PARTICLE SIZE (1=small,2=large)	I1
20-24	STATUS BYTES	5I1
25-444*	ELEMENT, ERROR PAIRS	30(F8.1, F6.0)

*ELEMENT, ERROR PAIRS IN THE FOLLOWING ORDER:

1. TOTAL MASS
2. ALUMINUM
3. SILICON
4. PHOSPHORUS
5. SULFUR
6. CHLORINE
7. POTASSIUM
8. CALCIUM
9. TITANIUM
10. VANADIUM
11. CHROMIUM
12. MANGANESE
13. IRON
14. NICKEL
15. COPPER
16. ZINC
17. GALLIUM
18. ARSENIC
19. SELENIUM
20. BROMINE
21. RUBIDIUM
22. STRONTIUM
23. CADMIUM
24. TIN
25. ANTIMONY
26. BARIUM
27. MERCURY
28. LEAD
29. QUALITY CONTROL, FRONT/BACK RATIO
30. QUALITY CONTROL, ARGON

UNITS:

TOTAL MASS - MICROGRAMS/CUBIC METER
ALL OTHERS - NANOGRAMS/CUBIC METER

Table 13. Interpretations of Status Words

10000	Mass data available.
01000	Front/Back ratio available for penetration correction.
00100	Fluorescer 1 data available.
00010	Fluorescer 2 data available.
00001	Fluorescer 3 data available.
11111	Complete data set for fine particles.
00000	Data not available for this slide.
10111	Complete data set for coarse particles.

REFERENCES

1. Loo, B.W., J.M. Jaklevic and F.S. Goulding. "Dichotomous Virtual Impactors for Large-Scale Monitoring of Airborne Particulate Matter," In: Fine Particles: Aerosol Generation, Measurement, Sampling and Analysis. B.Y.H. Liu, ed., Academic Press, New York, 1976. pp. 311-350.

2. Goulding, F.S., J.M. Jaklevic and B.W. Loo. "Fabrication of Aerosol Monitoring System for Determining Mass and Composition as a Function of Time." EPA-650/2-75-048 Environmental Protection Agency Report, Research Triangle Park, North Carolina, 1975.

3. Jaklevic, J.M., B.W. Loo and F.S. Goulding. "Photon-Induced X-Ray Fluorescence Analysis Using Energy-Dispersive Detector and Dichotomous Sampler," In: X-Ray Fluorescence Analysis of Environmental Samples. T.G. Dzubay, ed., Ann Arbor Science, 1977. pp. 3-18.

4. Jaklevic, J.M., D.A. Landis and F.S. Goulding. "Energy Dispersive X-Ray Fluorescence Spectrometry Using Pulsed X-Ray Excitation." Adv. X-Ray Analysis, 19:253, 1976.

5. Jaklevic, J.M., R.C. Gatti, F.S. Goulding and B.W. Loo. "Beta-Gauge Methods Applied to Aerosol Samples." Submitted to Environmental Protection Agency, Research Triangle Park, North Carolina, March 1980.

6. See References 1 and 2.

7. Whitby, K.T., R.B. Husar and B.Y.H. Liu. "The Aerosol Size Distribution of Los Angeles Smog." In: Aerosols and Atmospheric Chemistry, G.M. Hidy, ed., Academic Press, New York, 1972. pp. 237-264.

8. See References 3 and 4.

9. See Reference 4.

10. Jaklevic, J.M. and R.L. Walter. "Comparison of Minimum Detectable Limits Amoung X-Ray Spectrometers." In: X-Ray Fluorescence Analysis of Environmental Samples. T.G. Dzubay, ed., Ann Arbor Science, 1977. pp 63-75.

11. Schamber, F.H. "A Modification of the Linear Least-Squares Fitting Method Which Provides Continuum Supression." In: X-Ray Fluorescence Analysis of Environmental Samples. T.G. Dzubay, ed., Ann Arbor Science, 1977. pp. 241-257.

12. Russ, J.C. "Processing of Energy Dispersive X-Ray Spectra." X-Ray Spectrometry, 6:37, 1977.

13. Giauque, R.D., F.S. Goulding, J.M. Jaklevic and R.H. Pehl. "Trace Element Analysis with Semiconductor Detection X-Ray Spectrometers." Anal. Chem., 45:671, 1973.

14. Giauque, R.D., R.B. Garrett, and L.Y. Goda. "Calibration of Energy Dispersive X-Ray Spectrometers for Analysis of Thin Environmental Samples." In: X-Ray Fluorescence Analysis of Environmental Samples T.G. Dzubay, ed., Ann Arbor Science, 1977. pp. 153-164.

15. Loo, B.W., R.C. Gatti, B.Y.H. Liu, C.S. Kim and T.G. Dzubay. "Absorption Corrections for Submicron Sulfur Collected in Filters." In: X-Ray Fluorescence Analysis of Environmental Samples. T.G. Dzubay, ed., Ann Arbor Science, 1977. pp. 187-202.

16. Dzubay, T.G. and R.O. Nelson. "Self-Absorption Corrections for X-Ray Fluorescence Analysis of Aerosols." Adv. in X-Ray Anal., 18:619, 1975.

17. Dzubay, T.G. and P.J. Lamothe. "Polymer Film as Calibration Standards for X-Ray Fluorescence Analysis." Adv. in X-Ray Anal., 20:411-421, 1977.

18. Camp, D.C., A.L. Van Lehn, J.R. Rhodes and A.H. Pradzynski. "Intercomparison of Trace Element Determinations in Simulated and Read Air Particulate Samples." X-Ray Spectrometry, 4:123-127, 1975.

19. Camp, D.C., A.L. Van Lehn and B.W. Loo. "Intercomparison of Samplers Used in the Determination of Aerosol Composition." U.S. Environmental Protection Agency, Office of Research and Development Report EPA-600/7-78-118 (1978).